Hindawi
Advances in Civil Engineering
Volume 2019, Article ID 9084861, 9 pages
https://doi.org/10.1155/2019/9084861

Research Article

Feasibility of a Polymer Foaming Agent as a Grouting Material for Broken Coal Masses

Zhidong Sun,[1] **Junxiang Zhang**,[1,2] **and Yuning Sun**[1,2]

[1]*School of Energy Science and Engineering, Henan Polytechnic University, Jiaozuo 454003, China*
[2]*State and Local Joint Engineering Laboratory for Gas Drainage & Ground Control of Deep Mines, Henan Polytechnic University, Jiaozuo 454003, China*

Correspondence should be addressed to Junxiang Zhang; zhangjunxiang9@126.com

Received 7 September 2018; Revised 20 February 2019; Accepted 6 March 2019; Published 1 April 2019

Academic Editor: Patrick W. C. Tang

A new soluble polymer foaming (PF) grouting material was developed by using hydrophilic amino resin as the base material and adding other cross-linking, foam, foam stabilizing, toughening, and coupling agents. The PF material exhibited low viscosity, excellent adhesion, and strong penetration. The grouting reinforcement effect of the proposed PF material on broken coal masses was investigated and compared with that of traditional superfine cement (SC) through simulation experiments. Results showed that after grouting, fractures, joints, and other failure planes inside raw coal were filled and bonded, and the mechanical strength of the grout-coal concretion improved relative to the residual strength of raw coal. The average uniaxial compressive strength of SC specimens was 6.16 MPa, whereas that of PF specimens was 10.85 MPa. Moreover, the PF specimens presented an obvious characteristic of plastic strengthening. Analyzing the reinforcement effect of the grouting materials on the basis of single structural plane theory revealed that at the critical state, the average σ_3 value of SC specimens was 1.43 MPa, whereas that of PF specimens was 3.09 MPa. In addition, coordination between the lateral and axial deformations of the PF specimens during compression promoted the formation of a bearing structure that can adapt to deformation. This structure is crucial for the safe operation of coal mines.

1. Introduction

Fractures and joints develop in coal and rock masses under the action of extended geological evolution and engineering disturbance. The development of these fractures and joints results in the destruction of the integrity and continuity of coal and rock masses. When the initial stress state of the coal mass is disturbed by extractive activities, original fractures, joints, and other weak structural planes further develop, form numerous secondary fractures, and may even promote macrocracking. The drastic reductions in the bearing capacity of the fractured coal mass caused by these phenomena promote the occurrence of gas outburst, mine water inrush, and other geological disasters. Meanwhile, fractures in the coal body also provide oxygenated environments for coal oxidative heat storage, the main factor that leads to spontaneous coal combustion, which seriously affects the safety of underground mining activities [1–3]. Grouting reinforcement is an important method for improving the physical and mechanical properties of coal masses. The grouting material can be injected into the fracture network to fill and bond defects through the effect of pump pressure. Filling and bonding enhance the strength and stability of broken coal masses by increasing the occlusion strength of fracture surfaces and by bonding broken coal into a continuous mass [4–6].

Various grouting materials are currently used in coal production. Cement-based materials are the most widely used inorganic grouting materials. Nevertheless, ordinary cement blocks grouting channels during grouting and hinders the achievement of the ideal reinforcement effect, given its long solidification time and low early strength, as well as its high content of inorganic particles with average particle sizes of 60~100 μm [7, 8]. The application range of

ordinary cement can be extended by grinding cement into superfine particles with sizes of 5~20 μm; however, the large-scale application of superfine cement (SC) is hampered by its high reactivity, short storage period, and tendency to cake in moist environments [9, 10]. The use of organic grouting materials has expanded with their continuous development and improvement. Polyurethane, a representative of organic materials, is produced by reacting polyester polyol with polyisocyanate. It is widely used because of its short curing time and high foaming coefficient; however, its high foaming speed and viscosity prevent its full diffusion in strata [11–13]. Although other organic materials, such as epoxy and phenolic resins, have high mechanical strength and strong thermal stability, they are insoluble in water and thus must be diluted with specific diluents before use; this requirement increases their cost [14–16]. Therefore, novel grouting materials with low cost and superior performance should be explored to promote safe coal production and to address the problems of air leakage, water inrush, and coal spontaneous combustion in coal mines.

To solve the shortcomings of currently available grouting materials, a new polymer foaming (PF) grouting material with low viscosity, excellent adhesion, and strong penetration was developed in this study. This PF material was prepared using hydrophilic amino resin as the base material and adding other cross-linking, foam, foam stabilizing, toughening, and coupling agents. Grouting simulation experiments were conducted using a traditional SC material and the proposed PF material. The grouting reinforcement effects of the two materials on broken coal masses were compared, and the reinforcement mechanism of the PF material was also analyzed from the perspectives of micromorphology and micromechanics. The results of this study are expected to provide a reference for the popularization and application of PF materials.

2. Material Preparation and Experimental Scheme

2.1. Material Preparation. Amino resin, a modified urea-phenol-formaldehyde resin, was used as the base material for the PF material because it has good hydrophilicity and strong cohesion that result from its high hydroxymethyl and amide group contents. The resin molecule can undergo polycondensation in the presence of a cross-linking agent and transforms from a chain structure to a three-dimensional network structure. The foaming agent was a type of carbonate, which contains CO_3^{2-} ions and can react with H^+ ions in the grout to produce CO_2 as the expansion gas source for the volume expansion of the material. Span-80 was used as a foam stabilizer to reduce the surface tension of the grout system and enhances the strength of bubbles if material expansion is affected by the merging or collapse of the bubbles. The toughening agent, PEG-6000, was a hydrophilic flexible polymer material that improves the material's toughness and impact properties by embedding its long molecular chain into the resin molecule during resin matrix curing. The coupling agent selected KH-560, which possesses bifunctional groups; among these groups, organic functional groups with strong affinity can react with the long molecular chains of the resin; hydrolytic groups can react with the hydroxyl groups of the injected coal to form hydrogen bonds or initiate dehydration to form ether bonds. Bond formation subsequently triggers the coupling of heterogeneous materials and improves the reinforcement effect of the PF materials on the broken coal.

The optimum proportion of each component of the PF material was determined on the basis of extensive experiments and field tests:

$$\begin{aligned} &\mathrm{m\,(resin)} : \mathrm{m\,(cross\text{-}linking\ agent)} : \mathrm{m\,(foaming\ agent)} \\ &\quad : \mathrm{m\,(foam\ stabilizer)} : \mathrm{m\,(toughening\ agent)} \\ &\quad : \mathrm{m\,(coupling\ agent)} = 1.0 : 0.02 : 0.01 : 0.01 : 0.03 : 0.01. \end{aligned} \tag{1}$$

The synthesis procedure of the PF material was as follows: first, weighing a certain amount of amino resin in the agitator, and then, an appropriate amount of distilled water was added for stirring; secondly, foaming, foaming stabilizer, toughening, and coupling agent were added in proportion for mixing to prepare the mixed solution; finally, mixing with the cross-linking agent to obtain the grout of the PF material.

In the experiments, SC produced by Henan Jutailong Co., Ltd. was selected as the traditional grouting material for comparison. The specific surface area and average diameter of the SC material were 800 m^2/kg and 5 μm, respectively. The basic chemical compositions of the material are listed in Table 1.

The main performance parameters of the traditional SC material and the proposed PF material used in the experiments are shown in Table 2.

2.2. Experimental Procedures. Grouting simulation experiments were conducted using a grouting simulation device, as shown in Figure 1(c). SC and PF materials were used as grouting to reinforce broken coal masses, and the grouting reinforcement effect of the PF material was compared with that of the SC material.

The grouting simulation device included an agitation vat, a grouting pump, a grouting gage, a grouting pipe, and a test chamber. First, pulverized coal with a particle size of 1–5 mm was loaded into the test chamber and compacted in layers to simulate an injected coal seam. Second, sealing rings were inserted between the flange plates at the two ends of the test chamber and fixed with screws. The grouting material was mixed with sufficient water in an agitation vat and then injected in the test chamber by a grouting pump. Pressure was controlled at 0.5 MPa during grouting. After completing the grouting operation, the test chamber was stored for 7 days and then dismantled to remove the grout-coal concretion, which was processed into standard cylindrical specimens with diameters of 50 mm and lengths of 100 mm, as shown in Figure 1(e), for experimental analysis.

2.3. Experimental Methods. The uniaxial compressive tests of raw coal and the different grouting reinforced specimens were by the RMT-150B electrohydraulic servo test machine, the displacement control method was adopted in the

Table 1: The chemical composition of the SC material.

Component	CaO	SiO_2	Al_2O_3	F_2O_3	MgO	SO_3	Alkali content	Loss on ignition
Mass percentage	54.94	26.74	8.25	3.04	2.19	2.09	0.59	1.37

Table 2: Main performance parameters of different materials.

Material	Material-water ratio	Apparent viscosity (MPa·s)	Gel time (h)	Volumetric change
SC	1 : 1.0	337	8.97	Shrinking rate of 23.7%
PF	1 : 1.0	81	0.67	Expansion rate of 9.29%

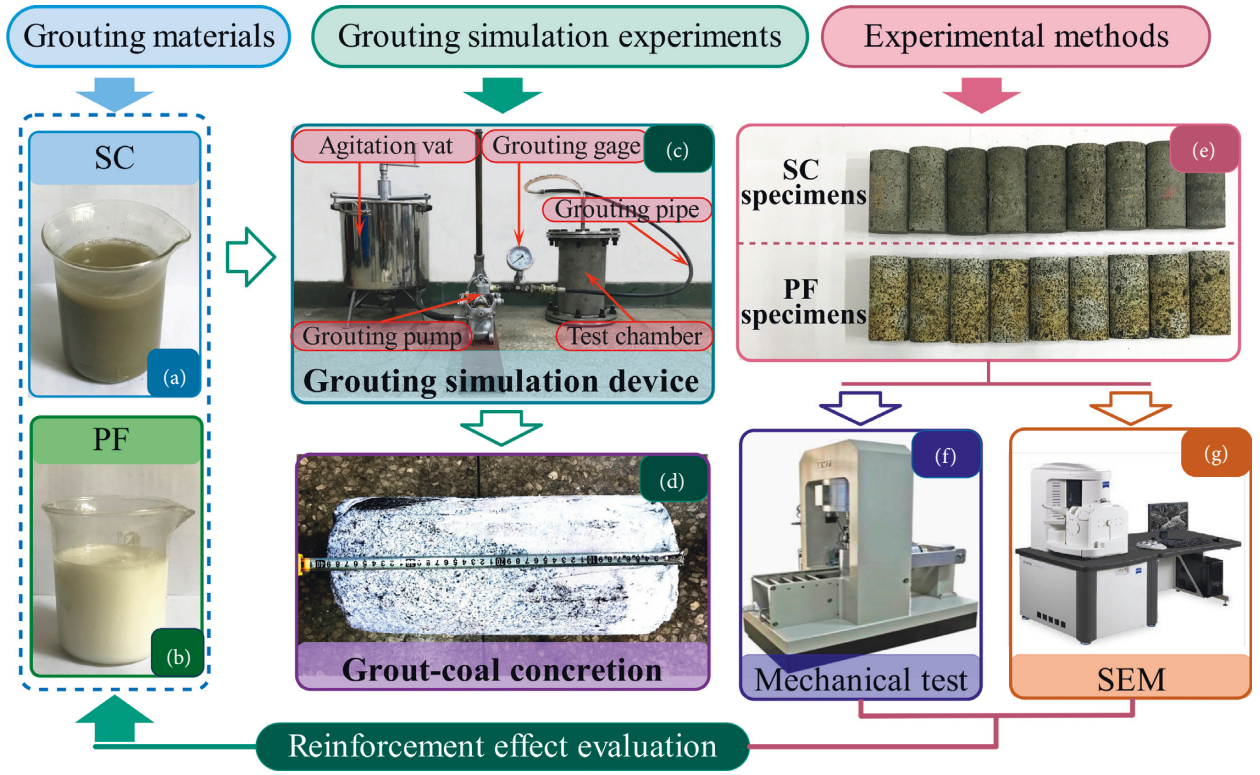

Figure 1: Experimental procedures.

experiments, the specimens were loaded with the speed of 0.02 mm/s until damage, and the 5 mm displacement sensor was used to measure the axial displacement, and the 1000 kN stress sensor was used to measure the axial load. In the tests, four specimens were set for each group, and the PF and SC grouting reinforced specimens were taken from their respective grout-coal consolidation to ensure that the experimental condition for each group of grouting reinforced specimens was consistent.

The JSM-6390/LV scanning electron microscope (SEM) was used to observe the microstructure of raw coal and the different grouting reinforced specimens, which can magnify images 5~300000 times and the resolution of 3.0 nm at an acceleration voltage of 0.5~30 kV.

3. Analysis of Experimental Results

3.1. Analysis of the Grouting Reinforcement Effect. The uniaxial compressive tests of the raw coal and the different grouting reinforced specimens were conducted in accordance with the standard of GB/T 23561–2010 Methods for determining the physical and mechanical properties of coal and rock [17], and the results are listed in Tables 3 and 4.

As shown in Table 3, the uniaxial compressive strength of raw coal is relatively high and can reach an average value of 11.86 MPa. The residual strength of raw coal, however, is low and has an average value of 0.62 MPa. After grouting, broken coal particles and failure planes in the coal mass are continuously integrated through bonding by different degrees. Thus, bonding increases the strength of the concretion relative to the residual strength of the raw coal. Table 4 indicates that after grouting with the traditional SC material, the average uniaxial compressive strength and strength recovery coefficients of SC specimens are 6.16 MPa and 0.52, respectively. By contrast, the average uniaxial compressive strength and strength coefficients of PF specimens are 10.85 MPa and 0.91, respectively. Mechanical test results show that the reinforcement effect of the PF material on

Table 3: Uniaxial compressive test results of raw coal specimens.

Specimen	D (mm)	H (mm)	σ_c (MPa)	σ_c^* (MPa)	$\overline{\sigma_c}$ (MPa)	$\overline{\sigma_c^*}$ (MPa)
RC-1	49.7	99.8	10.61	0.55	11.86	0.62
RC-2	49.9	100.1	13.45	1.01		
RC-3	49.5	99.7	11.16	0.29		
RC-4	49.7	101.2	12.20	0.64		

Note: σ_c is the uniaxial compressive strength, $\overline{\sigma_c}$ is the average uniaxial compressive strength, σ_c^* is the residual strength, and $\overline{\sigma_c^*}$ is the average residual strength.

Table 4: Uniaxial compressive test results of different grouting reinforced specimens.

Grouting material	Specimen	D (mm)	H (mm)	σ_c (MPa)	σ_c^* (MPa)	Strength recovery coefficient
SC	SC-1	49.8	100.1	7.26	6.16	0.52
	SC-2	49.4	99.7	5.99		
	SC-3	49.7	99.9	6.31		
	SC-4	49.5	100.2	5.09		
PF	PF-1	49.6	100.1	12.01	10.85	0.91
	PF-2	49.5	100.2	10.99		
	PF-3	49.3	99.8	9.80		
	PF-4	49.7	100.1	10.58		

Note: strength recovery coefficient is the ratio of the concretion's uniaxial compressive strength to the raw coal's uniaxial compressive strength.

broken coal masses is superior to that of the traditional SC material.

3.2. Analysis of Stress-Strain Curves and Failure Characteristics. The stress-strain curves and failure characteristics of raw coal and specimens reinforced with different grouting materials are shown in Figure 2. According to the achievements of reference [18, 19] that universal regularity of stress-strain curves on coal and solid materials, the failure process of each specimen can be divided into five different stages: (I) OA—initial compaction stage, (II) AB—linear elastic stage, (III) BC—yield stage, (IV) CD—strain softening stage, and (V) DE—residual strength stage. The initial compaction stage involves the gradual closure of the original pores and fractures in the specimens; during this stage, the stress-strain curves appear concave. This stage is followed by the linear elastic stage, wherein stress varies linearly with strain, and a small amount of microfractures develop in the specimens. As load increases, the specimens begin to yield and exhibit plastic deformation and fracture formation. The stress peaks at point C. Then, during the strain softening stage, the fractures continually propagate and coalesce, and the bearing capacity of specimens decreases correspondingly. These phenomena result in macroscopic cracking that eventually leads to specimen failure. In the final residual strength stage, new fractures are no longer produced, and friction between the failure planes of the specimen is required to maintain a relatively low stress level.

Comparing the results shown in Figure 2 reveal that the ascending segment (I, II, and III) of the stress-strain curves of the raw coal specimen RC-3 rises smoothly without obvious fluctuation. This behavior indicates that raw coal is relatively dense with undeveloped original fractures. When the stress on RC-3 peaks, the specimen is destroyed rapidly and forms several splitting surfaces, and stress sharply decreases to the residual strength of 0.29 MPa. Thus, as shown in Figure 2(a), raw coal is destroyed through typical brittle failure.

However, the stress-strain curves of the SC-1 and PF-1 specimens exhibiting an "S" shape changed trend during phases I, II, and III. This result indicates that the specimens possess plastic-elastic-plastic deformation characteristics, and stress then declines slowly in the postpeak stages (IV and V). Test results show that when stress reaches the peak value, the critical strains of SC-1 and PF-1 are 3.61 and 27.58, respectively. These data reveal that the plastic characteristics of the PF grout-coal concretion is more pronounced than that of the SC grout-coal concretion. Given the low cohesive force of the SC material, the cement can easily separate from the coal mass during loading and thus hinders the SC from transferring and releasing energy. This effect results in the small deformation of the SC specimen and shear failure along these weak cement planes, and Figure 2(b) shows that the SC-1 specimen presents a shear failure surface. Furthermore, the SC grouting material contains massive inorganic particles, which are difficult to inject into microfractures in the coal mass. Therefore, stress easily concentrates on unfilled areas under external force. And stress concentration also reduces the bearing capacity of the grout-coal concretion and accelerates the destruction of the SC specimen.

PF material is a true solution grout that lacks any suspended particles that easily penetrates fractures, joints, and other failure planes in broken coal mass. In addition, the resin matrix contains many active groups with excellent adhesion. These active groups increase the occlusal force between fracture surfaces and improve the mechanical stability of the injected coal mass. Therefore, the axial deformation of the PF specimen is large during compression, and stress negligibly decreases after reaching peak strength

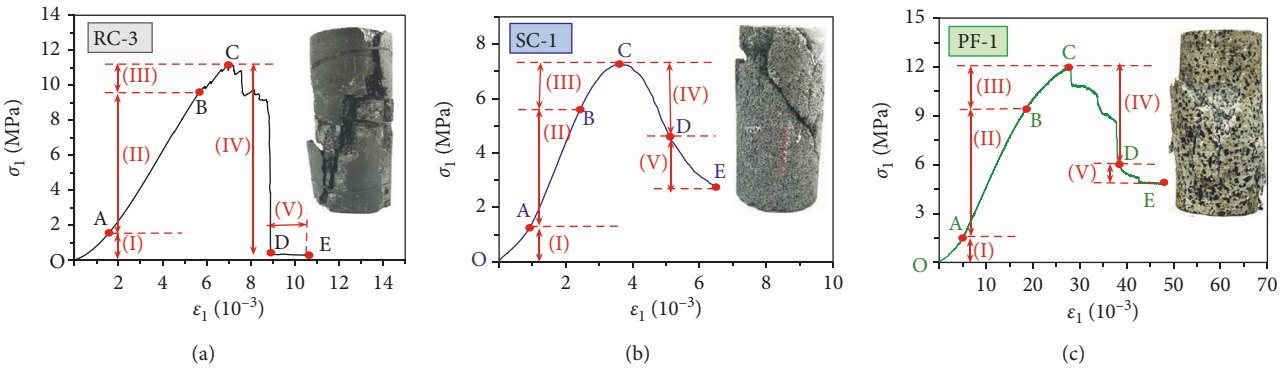

Figure 2: Uniaxial compression test results of different grouting reinforced specimens: (a) raw coal, (b) SC, and (c) PF.

but maintains a relatively high residual strength level with good structural integrity. The failure curve of PF-1 in Figure 2(c) shows that PF-1 has a plastic strengthening characteristic.

Comparing the stress-strain curves and the failure types of the pre- and postgrouted coal reveals that the raw coal shows brittle failure and is easily destroyed with small deformation. Meanwhile, the grouted concretion, particularly the PF concretion, presents different degrees of plastic deformation characteristics. In practical engineering applications, this plastic strengthening characteristic improves coal stability by participating in energy transfer and release and enables the postgrouted coal to adapt to deformations.

4. Analysis of the Mechanism Underlying Grouting Reinforcement

4.1. Theoretical Analysis Based on Single Structural Plane Theory. In the single structural plane theory, which was proposed by Jaeger [20], a single structural plane AB is assumed to exist in the coal rock mass. β is the angle between the AB plane and the maximum principal stress direction. The strength analysis of the single structural plane AB is shown in Figure 3.

The decrease in the uniaxial compressive strength of the coal specimen is caused by tensile failure inside the coal mass. Thus, the failure plane of the coal specimen should conform to the following conditions:

$$\beta < \beta_1 \text{ or } \beta > \beta_2, \tag{2}$$

where β is the structural plane angle of raw coal, °; β_1 and β_2 are the failure plane angles of raw coal, °.

Although failure planes inside the broken coal mass can be bonded after grouting, they remain as weak structural planes in the concretion. Therefore, the failure of the concretion specimen under uniaxial compression can be regarded as failure along these structural planes. Accordingly, the failure plane angle of the concretion should satisfy the following equation:

$$2\beta_2' < 2\beta' < 2\beta_1', \tag{3}$$

where $\beta\prime$ is the structural plane angle of concretion,°; β_1' and β_2' are the failure plane angles of concretion,°.

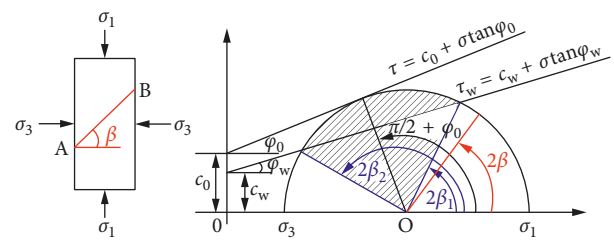

Figure 3: Strength theory analysis of single structural plane.

Considering that the structural plane of the concretion is the failure plane of raw coal before grouting, that is, $\beta\prime = \beta$, the following relationship exists:

$$\begin{aligned} \beta_1' &\neq \beta_1, \\ \beta_2' &\neq \beta_2. \end{aligned} \tag{4}$$

Failure planes in the broken coal mass can be filled and bonded through grouting. Therefore, the movement of the internal block inside the coal is restricted, and the stress state of the postgrouted coal transforms biaxial stress into the triaxial stress. Thus, $\sigma_3 \neq 0$. Based on the sine theorem, the failure plane angle should satisfy the following relation:

$$\frac{(\sigma_1 - \sigma_3)/2}{\sin\ \varphi_w} = \frac{c_w \cot\ \varphi_w + ((\sigma_1 + \sigma_3)/2)}{\sin(2\beta_1' - \varphi_w)}, \tag{5}$$

where c_w is the cohesive force of the structural plane inside the raw coal, MPa; φ_w is the internal friction angle of the structural plane inside the raw coal, °; σ_1 is the axial stress, MPa; and σ_3 is the lateral stress, MPa.

By simplifying equation (5), the failure plane angle can be obtained as follows:

$$\beta_1' = \frac{\varphi_w}{2} + \frac{1}{2}\arcsin\left[\frac{(\sigma_1 + \sigma_3 + 2c_w \cot\ \varphi_w)\sin\ \varphi_w}{\sigma_1 - \sigma_3}\right]. \tag{6}$$

Assuming that $\beta = \beta_1'$, the lateral stress (σ_3) of the grout-coal concretion at the critical state can be calculated as follows:

$$\sigma_3 = \frac{[\sin(2\beta_1' - \varphi_w) - \sin\ \varphi_w]\sigma_1 - 2c_w \cot\ \varphi_w}{\sin(2\beta_1' - \varphi_w) + \sin\ \varphi_w}. \tag{7}$$

The shear parameters of the coal structural plane can be obtained by subjecting the raw coal specimens to the shear

test. The failure plane angle of raw coal at pregrouting is 69.4°, and the cohesive forces and internal friction angle are 0.57 MPa and 26.16°, respectively. Therefore, the value of σ_3 at the critical state can be calculated on the basis of the uniaxial compressive strength (σ_1) of the specimens, as shown in Table 2. The calculated results of σ_3 are listed in Table 5.

As shown in Table 5, at the critical state, the average σ_3 value of the SC specimens is 1.43 MPa, whereas that of the PF specimen is 3.09 MPa, which is 2.16 times that of the SC specimen. The results of theoretical analysis reveal that the lateral restraint effect of the PF material on broken coal is greater than that of the SC material.

4.2. Analysis of the Grout-Coal Interface. After the mechanical experiments, the grout-coal interfaces on the fracture surfaces of PF and SC samples were observed by SEM to analyze the reinforcement effect of different grouting materials on the broken coal mass. Figure 4(a) shows the SEM results for the SC concretion. Although many hexagonal $Ca(OH)_2$ crystals formed in the SC material, few high-strength aciculate AFt crystals formed. In addition, several cracks are present in the material. These cracks are attributed to the drying shrinkage of the cement-based material and result in the loose structure and low bonding strength on the grout-coal interface. Consequently, these interfaces easily dislocate and separate under an external load, and the movement of the coal block is difficult to restrain. Thus, the interfaces form weak structural planes in the concretion. These weak structural planes, in turn, cause the destruction of the concretion. Through the above analysis, we can conclude that the SC material has an extremely limited grouting reinforcement effect on broken coal masses.

Figure 4(b) shows the SEM results for the PF concretion. It shows that abundant colloidal particles are distributed in the resin matrix and are interlaced into a dense network structure. Given the special structure of the resin matrix, the colloidal particles continuously compress, yield, and dislocate during loading to transfer stress and dissipate energy. These behaviors may account for the plastic deformation characteristic of the PF concretion. Moreover, the structural characteristic of the grout-coal interface inside the PF concretion is dense without any cracks because the numerous cohesive active groups contained by the resin matrix tightly attach the PF material to the surface of the coal and bond loose coal as a continuous whole. By comparison, it is clear that the PF material exerts a superior reinforcement effect on the broken coal mass.

4.3. Analysis of Deformation Coordination. Comparing the ε_3–ε_1 curves of pre- and postgrouted coal, as shown in Figure 5, shows that the lateral strain of raw coal specimen RC-3 is low during the initial compaction stage (I) and elastic deformation stages (II), whereas its axial strain increases rapidly. Thus, the $\varepsilon_3/\varepsilon_1$ ratio of RC-3 is low. In the yield stage (III), the lateral strain of RC-3 increases quickly. This behavior increases the $\varepsilon_3/\varepsilon_1$ ratio of the specimen. The raw coal undergoes uncoordinated deformation at this stage. Uncoordinated deformation leads to the rapid formation of macrofailure planes in the coal specimen, reduces coal-bearing capacity, weakens lateral restraint between failure planes, and accelerates the destruction of the coal specimen. The internal block of raw coal can slip along these planes and increase the lateral strain of the coal specimen with the continuous development of failure planes inside the coal mass during the postpeak stages (IV and V) until the coal specimen is destroyed.

Table 5: The calculated results of σ_3 at the critical state.

Grouting material	Specimen	σ_1 (MPa)	σ_3 (MPa)	$\overrightarrow{\sigma_3}$ (MPa)
SC	SC-1	7.26	1.82	1.43
	SC-2	5.99	1.37	
	SC-3	6.31	1.48	
	SC-4	5.09	1.05	
PF	PF-1	12.01	3.49	3.09
	PF-2	10.99	3.16	
	PF-3	9.80	2.71	
	PF-4	10.58	2.99	

The concretion specimen reinforced with SC possesses a certain plastic characteristic, as shown in Figure 5(b). The $\varepsilon_3/\varepsilon_1$ ratio of the SC-1 specimen is vanishingly low in the phases I and II. This behavior indicates that the SC specimen is in a state of constant compression. When stress reaches the peak value, the $\varepsilon_3/\varepsilon_1$ ratio of the specimen increases gradually, and the specimen begins to yield. As the load continues to increase, the $\varepsilon_3/\varepsilon_1$ ratio of the SC specimen markedly increases. Moreover, the SC specimen undergoes uncoordinated deformation, which accelerates the formation of cracks that eventually lead to the complete destruction of the specimen.

However, after grouting with the PF material, the broken coal mass exhibits remarkably improved stability and plastic strength. Figure 5(c) shows that the lateral strain of the PF specimen increases uniformly during loading. The $\varepsilon_3/\varepsilon_1$ ratio of the PF specimen is low and increases almost linearly in the ascending segments (I, II, and III). The specimen undergoes uniform deformation over a wide deformation range. This behavior is conducive for the maintenance of high stability and strong plasticity and the formation of a bearing structure that can adapt to the deformation of the surrounding rock. The PF material can directly fill the fracture network inside the broken coal mass to enhance the strength of the fracture surfaces, given its low viscosity and strong cohesiveness. Meanwhile, it can strengthen friction and occlusion between fracture surfaces through penetration. By restraining the movement and changing the force-transferring mechanism of failure planes, the lateral deformation of the coal block can be limited. Accordingly, the PF concretion undergoes coordinated two-dimensional deformation and improves the mechanical strength and stability of the concretion.

After the uniaxial compressive tests, the fracture surfaces of PF and SC specimens were taken as samples for microscopic observation to analyze the deformation characteristics of different specimens. Figure 6(a) displays the micromorphology of the SC specimen. A fracture with an aperture of approximately 5 mm inside the coal mass is not

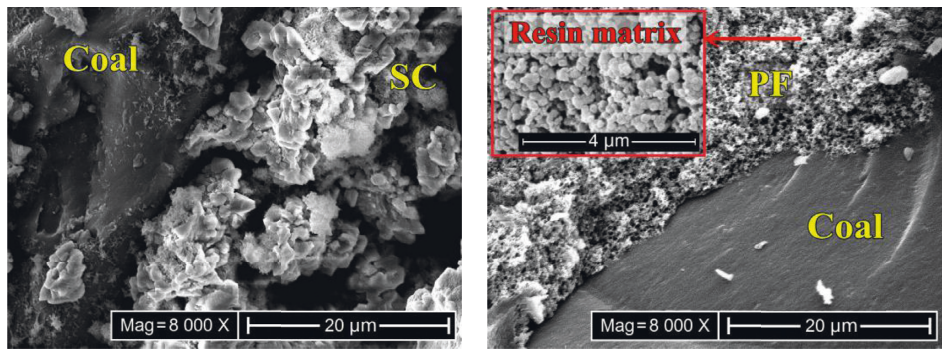

(a) (b)

Figure 4: Grout-coal interface of different specimens: (a) SC and (b) PF.

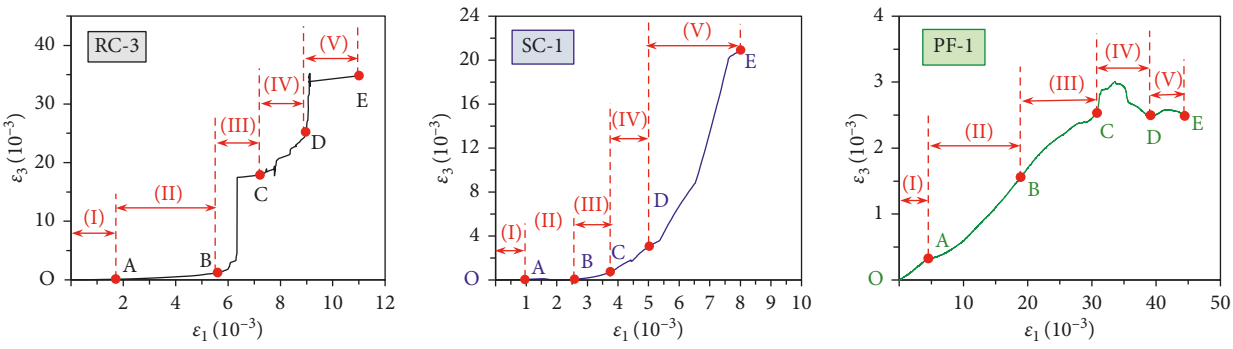

(a) (b) (c)

Figure 5: ε_3–ε_1 curves of coal before and after grouting: (a) raw coal specimen, (b) SC specimen, and (c) PF specimen.

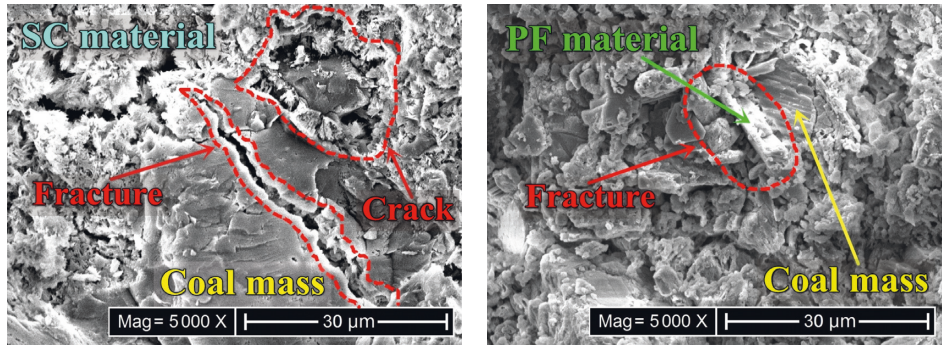

(a) (b)

Figure 6: Microstructure of different grouting reinforced specimens: (a) SC and (b) PF.

filled by the SC material because the filling effect is closely related to the particle size of the grouting material. Considering that the SC material is granular, it cannot easily penetrate the fracture channels, which is less than three times its particle size [21]. Therefore, the SC material cannot achieve the ideal grouting effect on microfractures. In addition, the existence of cracks between the SC and coal can be attributed to the high bleeding ratio of the cement material, which results in a certain degree of volume shrinkage during cement solidification and gives rise to the separation between the SC material and coal surface.

However, the self-developed PF material is a solution-grout material that can easily penetrate into the microfractures of coal mass under pump pressure. Figure 6(b) shows the PF concretion without any obvious gaps. Fractures or cracks are fully filled by the PF material and form a space network that encapsulates loose coal particles in the stratum. These effects mimic the generation of new

composite materials with the PF material as the skeleton and broken coal as the aggregate. Consequently, the broken coal mass is rebonded as a continuous whole, and the destruction of the broken coal mass is prevented. Thus, reinforcement with the PF material improves the stability and bearing capacity of the broken coal mass.

5. Discussion

Engineering practice and relevant experiments demonstrate that the integral stability of the coal mass is closely related to fracture development and spatial distribution. Moreover, fracture evolution, extension, and connection are the root causes of coal destruction. However, these fractures and joints are the channels through which grouting materials can be injected to provide reinforcement.

In contrast to the traditional SC material, the PF material presents the characteristics of low viscosity, excellent adhesion, and strong penetration. These characteristics promote the filling and bonding of massive fractures inside the coal mass to effectively enhance the static and sliding friction between fracture surfaces or failure planes. This effect restricts the lateral movement of the coal block in the grouting area and weakens stress concentration at the crack tip. Therefore, the integrity, stability, and mechanical strength of the broken coal mass can be greatly improved through reinforcement with the PF material. Moreover, numerous active groups, such as hydroxymethyl ($-CH_2OH$), in the resin matrix of the PF material can associate with the mineral components of the broken coal mass to produce ionic or covalent bonds that further improve the reinforcement effect of the PF material [22], as shown in Figure 7, the action mechanism between PF material and coal mass. Hence, the complex stress-strain relationship presented by PF reinforced specimens under uniaxial compression result from the mutual coupling between the PF material and coal. PF-coal coupling, in turn, limits the development and expansion of failure planes, improves the mechanical strength of the inject coal mass, and transforms the failure mechanism of the concretion.

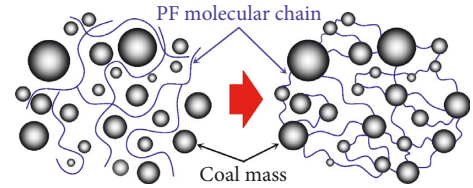

Figure 7: Action mechanism between PF material and coal mass.

6. Conclusion

(1) A new soluble PF material for grouting reinforcement of underground broken coal was developed, which used hydrophilic amino resin as a binder, and added several other additives, such as cross-linking, foaming, foam stabilizing, toughening, and coupling agents.

(2) Simulation experiments were conducted. In the simulations, the broken coal masses were reinforced with the traditional SC material or the proposed PF material. The results of mechanical tests indicate that after grouting, the fractures, joints, and other failure planes in raw coal bonded, and the strength of the concretion was greatly improved. The average uniaxial compressive strength and strength recovery coefficients of the SC specimens were 6.16 MPa and 0.52, respectively, whereas those of the PF specimens were 10.85 MPa and 0.91, respectively.

(3) Failure planes inside the coal mass were filled and bonded after grouting. The stress state of the coal mass transformed from biaxial stress to triaxial stress, which restrained the lateral movement of the coal block. Analyzing the grouting reinforcement effect on the basis of the single structural plane theory showed that at the critical state, the average value of σ_3 of SC specimens was 1.43 MPa, whereas that of the PF specimens was 3.09 MPa. These data indicate that the grouting reinforcement effect of the PF material is superior to that of the traditional SC material.

(4) The analysis of the ε_3–ε_1 curves of pre- and postgrouted coal shows that the mechanical properties of the grout-coal concretion changed from brittle failure to ductile failure, which can transfer and release energy under an external load. In contrast to the SC concretion, the PF concretion shows plastic strengthening characteristic, and its lateral and axial deformations tend to coordinate and result in the formation of a bearing structure that adapts to deformation. This structure allows the reinforced coal mass to remain stable.

Data Availability

The data used to support the findings of this study are available from the corresponding author upon request.

Conflicts of Interest

The authors declare that they have no conflicts of interest.

Acknowledgments

This study was supported by the National Natural Science Foundation of Youth Science Fund Project (no. 51604096), Plan for Scientific Innovation Talent of Henan Province (no. 164200510002), and Key Research Project of Higher Education Institution of Henan Province (no. 15A440002).

References

[1] L. Chen, E. Y. Wang, J. C. Ou, and J. W. Fu, "Coal and gas outburst hazards and factors of the No. B-1 coalbed, Henan, China," *Geosciences Journal*, vol. 22, no. 1, pp. 171–182, 2018.

[2] C. Wang, S. Yang, D. Yang, X. Li, and C. Jiang, "Experimental analysis of the intensity and evolution of coal and gas outbursts," *Fuel*, vol. 226, pp. 252–262, 2018.

[3] W. Zhao, Y. Cheng, P. Guo, K. Jin, Q. Tu, and H. Wang, "An analysis of the gas-solid plug flow formation: new insights into the coal failure process during coal and gas outbursts," *Powder Technology*, vol. 305, pp. 39–47, 2017.

[4] Z. Wang, L. Li, and C. Y. Wang, "Experimental study on failure of cracked rock–like material after grouting reinforcement," *Journal of Central South University*, vol. 49, no. 4, pp. 957–963, 2018.

[5] X. F. Ao, X. L. Wang, X. B. Zhu, Z. Y. Zhou, and X. X. Zhang, "Grouting simulation and stability analysis of coal mine goaf considering hydromechanical coupling," *Journal of Computing in Civil Engineering*, vol. 31, no. 3, article 04016069, 2017.

[6] X. L. Wang, Q. R. Qin, and C. H. Fan, "Research on comprehensive evaluation for grouting effect of broken and soft floor," *Arabian Journal of Geosciences*, vol. 10, no. 19, p. 420, 2017.

[7] A. P. Silva, A. M. Segadães, D. G. Pinto, L. A. Oliveira, and T. C. Devezas, "Effect of particle size distribution and calcium aluminate cement on the rheological behaviour of all-alumina refractory castables," *Powder Technology*, vol. 226, no. 8, pp. 107–113, 2012.

[8] L. Holzer, R. J. Flatt, S. T. Erdoğan, J. W. Bullard, and E. J. Garboczi, "Shape comparison between 0.4–2.0 and 20–60 μm cement particles," *Journal of the American Ceramic Society*, vol. 93, no. 6, pp. 1626–1633, 2010.

[9] E. Avci and M. Mollamahmutoğlu, "Permeability characteristics of superfine cement–grouted sand," *ACI Materials Journal*, vol. 114, no. 1, pp. 21–28, 2017.

[10] R. Xiao, Z.-c. Deng, and C. Shen, "Properties of ultra high performance concrete containing superfine cement and without silica fume," *Journal of Advanced Concrete Technology*, vol. 12, no. 2, pp. 73–81, 2014.

[11] Z.-X. Hu, X.-M. Hu, W.-M. Cheng, Y.-Y. Zhao, and M.-Y. Wu, "Performance optimization of one-component polyurethane healing agent for self-healing concrete," *Construction and Building Materials*, vol. 179, pp. 151–159, 2018.

[12] P. K. R. Vennapusa, Y. Zhang, and D. J. White, "Comparison of pavement slab stabilization using cementitious grout and injected polyurethane foam," *Journal of Performance of Constructed Facilities*, vol. 30, no. 6, article 04016056, 2016.

[13] Y. Wei, A. M. Asce, F. M. Wang, X. Gao, and Y. H. Zhong, "Microstructure and fatigue performance of polyurethane grout materials under compression," *Journal of Materials in Civil Engineering*, vol. 29, no. 9, article 04017101, 2017.

[14] S. Nadimi and K. Shahriar, "Experimental creep tests and prediction of long-term creep behavior of grouting material," *Arabian Journal of Geosciences*, vol. 7, no. 8, pp. 3251–3257, 2014.

[15] H. Xing, X. Yang, Y. Dang, X. Yao, and J. Zhou, "Experimental study of epoxy resin repairing of cracks in fractured rocks," *Polymers and Polymer Composites*, vol. 22, no. 5, pp. 459–466, 2014.

[16] L. M. Wu, Y. L. Yang, B. J. Liang, Y. Q. Huang, and J. J. Zeng, "Current research status of airtight plugging material used in the mine," *Guangzhou Chemistry*, vol. 41, no. 4, pp. 86–92, 2016.

[17] The National Standards Compilation Group of People's Republic of China, *GB/T 23561–2010 Methods for Determining the Physical and Mechanical Properties of Coal and Rock*, Standards Press of China, Beijing, China, 2010.

[18] M. Q. You, C. D. Su, and Y. Zhou, "Strength and deformation of specimen for different coal blocks and regression method of strength criterion," *Chinese Journal of Rock Mechanics & Engineering*, vol. 22, no. 12, pp. 2081–2085, 2003.

[19] S. J. Wang, W. C. Chen, and H. R. Fu, "Universal regularity of stress-strain curves on solid materials," *Journal of Engineering Geology*, vol. 25, no. 3, pp. 577–581, 2017.

[20] S. F. Guo, S. W. Qi, X. X. Li, Y. Zou, and S. S. Zhang, "Strength and deformation characteristics of rock sample with discontinuities under numerical uniaxial compression simulation tests," *Journal of Engineering Geology*, vol. 24, no. 5, pp. 891–898, 2016.

[21] P. Zhou, Q. D. Li, H. Li, and S. J. Li, "Advances in development of expendible lost circulation materials," *Oilfield Chemistry*, vol. 26, no. 1, pp. 111–114, 2009.

[22] J. Zhang, B. Li, and Y. Sun, "Performance of a new coal-dust-based composite sealing material for gas-drainage borehole," *Materials Express*, vol. 8, no. 4, pp. 325–334, 2018.